

Article

# The Grain for Green Project May Enrich the Mercury Concentration in a Small Karst Catchment, Southwest China

Rui Qu  and Guilin Han \* 

Institute of Earth Sciences, China University of Geosciences (Beijing), Beijing 100083, China; qurui@cugb.edu.cn

\* Correspondence: hanguilin@cugb.edu.cn; Tel.: +86-10-8232-3536

Received: 21 August 2020; Accepted: 24 September 2020; Published: 25 September 2020



**Abstract:** The Chinese project, better known as the Grain for Green Project (GGP), has changed the land-use type in the karst area of Puding county, Guizhou province, southwest China, and this study is aimed at evaluating the Hg distribution and determining factors in soils after the land-use change. A total of ten soil profiles were selected in the typical karst region, and the land-use types were divided into native vegetation land (NVL), farmland (FL), and abandoned farmland (AFL). Total Hg concentration under different land-use types increased in the order: NVL (average  $63.26 \mu\text{g}\cdot\text{kg}^{-1}$ ) < FL (average  $71.48 \mu\text{g}\cdot\text{kg}^{-1}$ ) < AFL (average  $98.22 \mu\text{g}\cdot\text{kg}^{-1}$ ). After agricultural abandonment for four to five years with a cover of native vegetation in the AFL, a higher concentration of Hg compared to the other two land-use types indicate that the Hg accumulation in soil results from vegetation restoration of AFL due to land-use change. Soil organic carbon (SOC) and macro-aggregates were highly correlated to Hg concentration in this study. Macro-aggregates can provide a stable condition for Hg due to the thin regolith and high porosity in the karst region. A high proportion of macro-aggregates can reduce the mobility of Hg in the karst area. Intense tillage can significantly reduce the formation of macro-aggregates in FL, but the macro-aggregates in AFL were recovered as well as those in NVL, resulting in the accumulation of Hg.

**Keywords:** mercury; Grain for Green Project (GGP); land-use change; soil organic carbon (SOC) and soil aggregate; karst soils; Southwest China

## 1. Introduction

Mercury (Hg) has been identified as a bioaccumulative and toxic contaminant due to its global distribution [1,2] and neurotoxic properties [3]. Inorganic Hg has an adverse effect on the normal metabolism of cells [4], while organic Hg can destroy brain function and cause cardiovascular diseases [5]. When brought into contact with plants, Hg can inhibit seed germination and decrease growth rates [6]. Elemental mercury emitted by natural processes and anthropogenic activities tends to be transported long-distance through the atmosphere, causing widespread problems like Minamata disease and negative effects on the intelligence of newborns [7–9]. In the natural environment, soil security was threatened by mercury deposition because of the rapid development of agriculture and industry [10–12]. The persistence, high toxicity, and bioaccumulation of heavy metals in the soil have become more and more significant hazards and cause adverse effects on the quality of soil and human health [13–16].

Soil organic carbon (SOC) and soil aggregates are taken into consideration as factors that influence Hg enrichment. Soil organic matter has significant importance because it not only retains nutrients but also pollutants in the soil [17]. Previous studies have reported a strong relationship between Hg and SOC [18,19], which is a significant binding agent for Hg in soil. SOC storage in the soil would

significantly change with the conversion of land-use types, such as deforestation, afforestation, and agricultural abandonment [20]. The stabilization of SOC is highly related to land-use change, tillage, and soil aggregates which determine the residence time of organic matter in the soil. Soil aggregates are a basic unit of soil structure and have a big influence in the SOC storage [21,22] and Hg in soil [23]. Furthermore, macro-aggregates can indicate land-use change because of its sensitivity [24] and reflect the influence of intense tillage in soil.

The largest karst region (~550,000 km<sup>2</sup>) is located in Southwest China [25–27]. The range of Hg concentration in the Chinese karst area is 27–20201 µg·kg<sup>-1</sup> at the topsoil and 25–60,001 µg·kg<sup>-1</sup> at the deep soil [28]. Ecosystems are highly fragile and vulnerable in the karst area due to frequent human activities like cultivation [29]. Long-term cultivation has caused severe soil erosion and nutrient loss in karst areas. With the low quality and steeply sloping farmland in the agricultural environment, many low-yielding farmlands have been abandoned due to the Grain for Green Project (GGP) [30]. The GGP is the largest forest ecological construction project in the world, aiming to improve the soil loss, desertification, and adverse effects of cultivation [30,31]. The program implemented the conversion of farmland into forest of about 14.67 million ha in 2010, successfully reducing runoff and soil erosion by land-use modification [32]. However, the GGP also has some adverse effects [33], like pollutant adsorption [34,35]. Therefore, the land-use change due to GGP in the karst area has motivated the interest of exploring the distribution characteristics of Hg after the abandoned farmland evolved into native vegetation land in this study. The objectives of this study were: (1) to evaluate the enrichment of Hg after the influences of GGP in the karst area and (2) to explore the influence of SOC and soil aggregates in Hg distribution under different land-use types in the karst area.

## 2. Materials and Methods

### 2.1. Study Area

The study area was located in Puding county (26°15′ to 26°16′ N, 105°46′ to 105°47′ E), which is a typical karst critical zone with a cover of 1.54 km<sup>2</sup> in Anshun city, Guizhou province, southwest China (Figure 1). The study area is dominated by a sub-tropical monsoonal climate, and the annual average temperature is approximately 15.1 °C, the annual average rainfall is approximately 1400 mm, and the rainy season is from May to October [36]. This region is surrounded by hills with slopes generally over 30° and an elevation of about 1310–1524 m.a.s.l. [37]. The main land-use types include dry farmland (55.65%), shrubland (23.35%), paddy land (14.39%), and secondary forest land (6.61%) in this catchment [38]. The range of soil layer thickness is 10 to 160 cm, with an average of 30 cm [39]. In the topsoil layer (0–30 cm), the primary mode of cultivation is plowing and crop rotation, including the urea and compound fertilizer applied in the farmland [40]. Intensive tillage was conducted in the study area resulting in severe soil degradation; thus, many farmlands were abandoned and turned into native vegetation land after the GGP [41]. Dolomite and limestone, primarily located on the hilltops and hillsides, were developing into calcareous soil first; then, the calcareous soil was transported into the central depression of the catchment and formed quaternary deposits according to a previous study conducted by Zhao et al. [41].

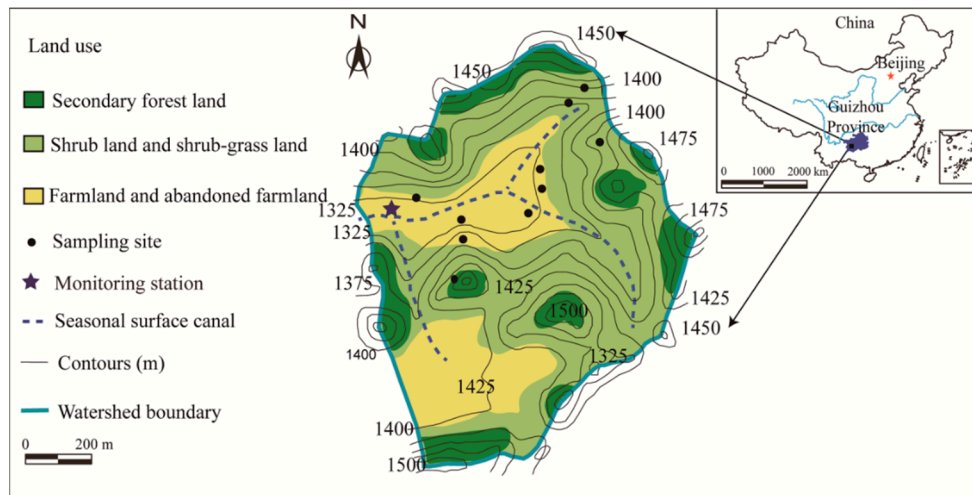


**Figure 1.** Land use and sampling sites of study area.

## 2.2. Sample Collection

To evaluate the influences of land-use change caused by GGP, sample collection in the study area was conducted in three different land-use types in June 2016. In total, three soil profiles from abandoned farmland (AFL), three soil profiles from farmland (FL), and four soil profiles from native vegetation land (NVL) (including three shrublands and one secondary forest land) were collected (Figure 1). The selection of locations was considered from paired sites, similar soil conditions, and the number of conversion years was clearly given or derived, aiming to compare the influence of GGP. The detailed information on land-use condition was described in Table 1, including the land-use change and dominant plant. The humus layer of NVL is black, loose, and has abundant plant roots. The soil profiles of FL and AFL are generally yellow and have a block structure. The collection of soil samples was done from bottom to top in each soil profile to avoid mixed pollution. The interval of the sample collection was 10 cm at 0–30 cm depth and 20 cm below 30 cm depth. The depth of each soil profile and data of each sample are shown in Table A1.

**Table 1.** The information on the land-use condition in three types stage.

Stage	Dominant Plant	Land-Use Condition
Native vegetation land (NVL)	<i>Eleusine indica</i> , <i>Ailanthus altissima</i>	Shrub-grass land and Mixed evergreen broadleaved deciduous forest
Farmland (FL)	<i>Arachis hypogaea</i> , <i>Zea mays</i>	Long-term cultivation activities, crop rotation, mixed application of fertilizer
Abandoned farmland (AFL)	<i>Oxalis corniculat</i> , <i>Eleusine indica</i>	Agricultural abandonment over 3–8 years, cover with shrubland or grassland

## 2.3. Sample Analysis Methods

The stones and coarse materials in soil samples were removed before being dried at room temperature (25 °C) by air. After being ground into powder, part of the dried samples was sieved through a 100-mesh sieve (<150 μm). Another part was unground for aggregates analysis. Diluted hydrochloric acid (HCl, 0.5 mol L<sup>-1</sup>) was used to soak soil samples for 24 h to remove inorganic carbonates [42–44]; then, the samples were treated using deionized water to make the supernatant liquid neutral. Soil organic carbon (SOC) was analyzed using an elemental analyzer (Vario TOC cube; Elementar, Langensfeld, Germany) after pretreatment [45,46]. For analysis of soil aggregates, the initial samples were uniformly separated into triplicate subsamples by quartering and macro-aggregates (250–2000 μm), micro-aggregates (53–250 μm), and silt and clay fraction (<53 μm) were separated by wet sieving [47]. The absolute content of Hg in soils, better known as total mercury (THg), was performed using an RA–915M mercury analyzer with the direct injection of a solid module (Lumex Instrument,

St. Petersburg, Russia) [48]. For the standard reference materials (GBW07402 and GBW07405) and parallel random samples, every ten soil samples were tested in order to ensure the accuracy of the analyzer. The standard reference materials were from the China National Standard Materials Research Center. The detection limit of the mercury analyzer is  $0.10 \mu\text{g}\cdot\text{kg}^{-1}$ . With adequate accuracy and precision, the mercury analyzer was fast and low cost without soil digestion, and had reduced losses of Hg during the pretreatment.

#### 2.4. Statistical Analysis

The data was analyzed by a two-tailed test among the THg, SOC, and proportion of aggregate size in each land-use type; the least significant difference was  $p < 0.05$ . Pearson correlation coefficient was performed at bivariate correlations to analyze the association among the THg, SOC, and proportion of aggregate size. The linear regression analysis using coefficient ( $R$ ) and  $p$ -values to describe the best-fit line express the relationships between variables. The data was carried out by SPSS 18.0 (SPSS Inc., Chicago, IL, USA) and Microsoft Office 2019 (Microsoft Corporation, Redmond, Seattle, WA, USA). The figures were constructed by SigmaPlot 12.5 (Systat Software GmbH, Erkrath, Germany) software package.

### 3. Results and Discussion

#### 3.1. Increased THg Concentration after Agricultural Abandonment

The data concerning THg in soils is presented in Appendix A Table A1, and the vertical distribution of THg is shown in Appendix A Figure A1. An overview of THg concentration, SOC concentration, and proportion of macro-aggregates under different types of land use is shown in Figure 2. THg concentration presents a visible increasing order among the three land-use types (Figure 2a). The THg concentration under abandoned farmland (AFL) is higher than that under the other land-use types. Generally, both farmland with an average THg concentration of  $71.48 \mu\text{g}\cdot\text{kg}^{-1}$  and native vegetation land with an average THg concentration of  $63.26 \mu\text{g}\cdot\text{kg}^{-1}$  are lower than the background Hg concentration ( $110 \mu\text{g}\cdot\text{kg}^{-1}$ ) in Guizhou province [49]. On the contrary, the THg concentration under abandoned farmland (average  $98.22 \mu\text{g}\cdot\text{kg}^{-1}$ ) is close to or little higher than the background value. Land-use change may play a key role in the enrichment of Hg in the soil according to relatively high Hg concentration in AFL. The GGP effectively changed the quality of soil, such as soil conservation, nutrient, and oxygen release [50,51]. Less soil and water loss may be a contributor to the enrichment of Hg in the abandoned farmland due to land-use change under GGP. The enrichment of Hg is a potential ecological risk for the forest; furthermore, when the AFL becomes FL again, the risk of Hg to public health will increase.

As for the SOC concentration and proportion of macro-aggregates, the characteristics of soil profiles under FL are significantly different from those under NVL and AFL. A possible explanation is that the highest SOC concentration under farmland is a result of anthropogenic input like agricultural activities with fertilizers (Figure 2b). Previous research has reported that land-use change under GGP in initial years led to the reduction of soil carbon [31,52]. This can probably be attributed to the soil loss from a change of land-use disturbance and lower degree recovery of vegetation [53,54].

Long-term tillage can impede the formation of macro-aggregates in the farmland [55]. For similar reasons, an intense tillage probably results in the lowest proportion of macro-aggregates under farmland (Figure 2c). After agricultural abandonment for years, the SOC concentration and macro-aggregates under abandoned farmland were recovered to a slightly similar level to that under native vegetation land. After the land-use change, the influence of tillage under AFL was gradually eliminated because SOC concentration and macro-aggregates need time to reach a new balance [45,56].

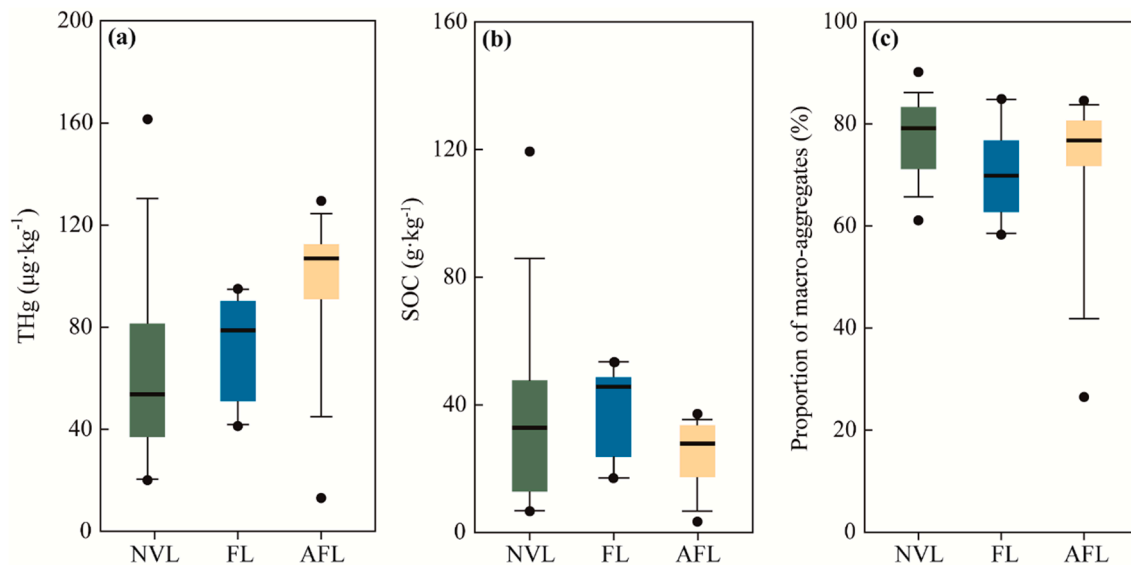


**Figure 2.** THg concentration (a), SOC concentration (b), and proportion of macro-aggregates (c) in soil profiles from NVL, FL, and AFL (o represents outliers). NVL: native vegetation land; FL; farmland; AFL: abandoned farmland.

### 3.2. Effects of SOC Concentration

Soil organic carbon plays a critical role in the Hg concentration in soil profiles. Ionic mercury tends to be combined with organic matter like humic acids and fulvic acids to be a more stable form [57]. Particular S-rich varieties have a high affinity for Hg in organic matter, resulting in the accumulation of Hg in soil [58,59]; thus, the SOC is beneficial for the soil mercury accumulation due to raising the adsorption of Hg [60]. SOC concentrations are generally expected to have high correlations with THg concentrations, thus are considered a controlling factor in the Hg cycle [61–63]. As shown in Figure 3, SOC concentration shows a significant correlation with THg concentration under all three different land-use types. The soil profile under FL has the highest SOC concentration, which is expected to have a higher THg concentration compared to those under the other two land-use types. However, the THg concentration in abandoned farmland is much higher than that in the other two types (Figure 2a). Therefore, not only the quantity but also the quality of SOC is related to soil or sediment samples [64–66]. A possible explanation is attributed to the special soil profile of the karst region. Previous studies have reported that soils in the karst region were characterized by thin regolith and high porosity due to surface and underground water flow [67,68]. Agricultural and soil microbial activities focus on the topsoils of the karst region [69]. The thin thickness of soil layers (average 30 cm) in the karst region probably enhances the influence of cultivation for the transport of Hg.

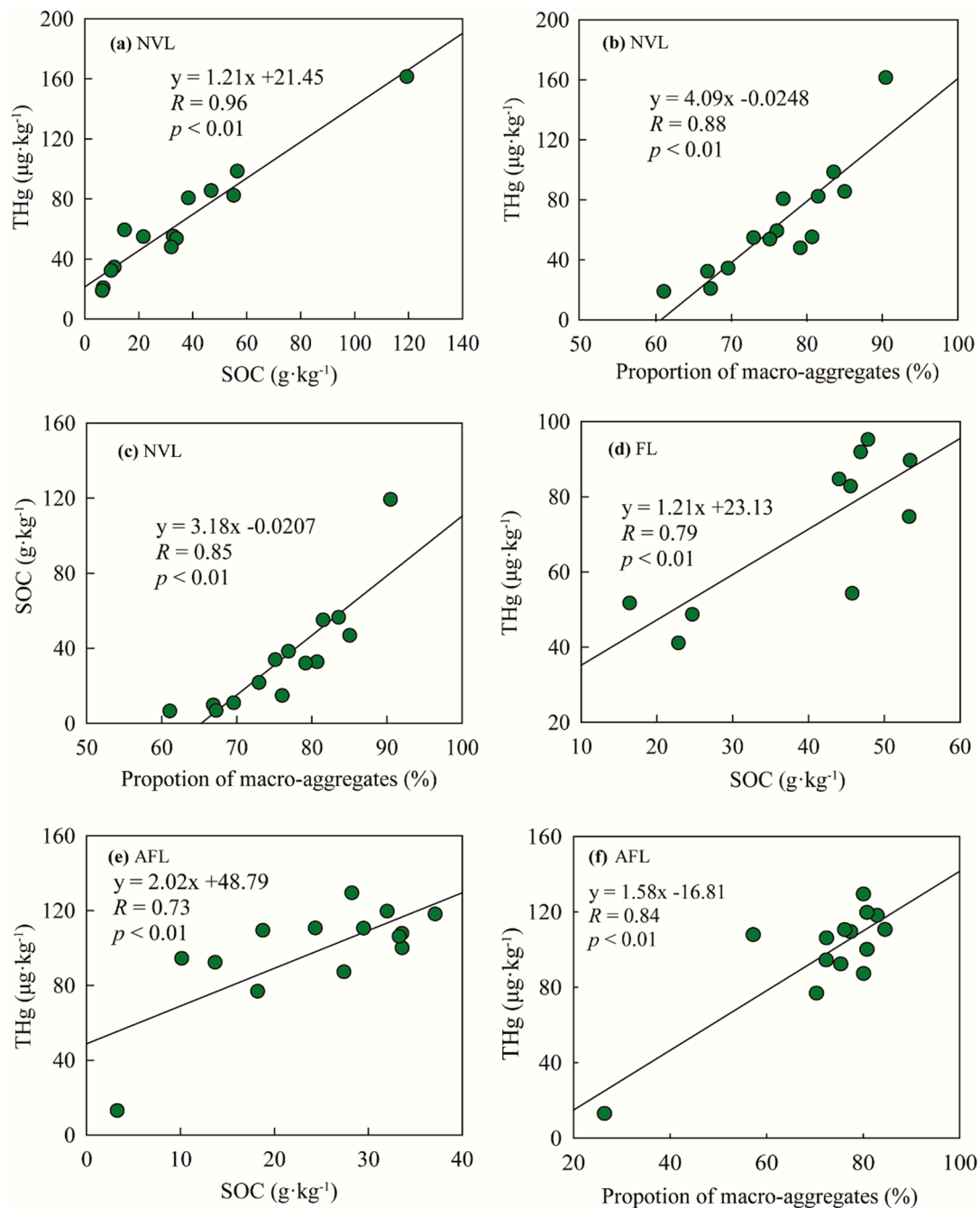


**Figure 3.** Line regression relationships between THg concentration, SOC concentration, and proportion of macro-aggregates. NVL: native vegetation land; FL: farmland; AFL: abandoned farmland.

### 3.3. Effects of Soil Aggregate Size on Hg Concentrations

With further study on the reason of Hg enrichment in abandoned farmland rather than farmland, soil aggregates are involved. Macro-aggregates are sensitive to the change in land management and reflect the effects of land-use change [70,71]. After agricultural abandonment, the plant biomass, enzyme, and soil microbial activity increase [72,73]. As significant organic binding agents, the soil microorganisms and plant debris play an essential role in the formation of macro-aggregates [24]. Hg mobility is probably reduced by this process, which enhances the binding between Hg and organic agents. As shown in Figure 3, THg concentration shows a high correlation with the proportion of macro-aggregates under NVL and AFL. Besides, the correlation between THg concentration with micro-aggregates and silt and clay is shown in Appendix A Figure A2. However, a previous study

reported that fine soil aggregate size showed higher THg concentration [23]. This result may be attributed to more new SOC in micro-aggregates than macro-aggregates. However, the new SOC probably decreases due to long-term cultivation activities in this study [45]. Furthermore, the aggregate hierarchy model proposed that the macro-aggregates formation wrap the OC-enriched fresh residues [55]; thus, micro-aggregates will be wrapped into macro-aggregates during the process of formation without disturbance of cultivation activities after agricultural abandonment. Visible differences in the distribution of aggregate size with a depth between native vegetation land and farmland show that tillage significantly reduces the macro-aggregate formation (Figure 4). The distribution pattern in abandoned farmland, which is similar to that in native vegetation land, indicates the gradual recovery from the influence of tillage. Less formation of macro-aggregates results in destroyed soil organic matter in micro-aggregates [47]. Soil aggregates protect the soil organic matter from microbial and enzymatic attack [74], resulting in more stable bonding between Hg and organic matter.

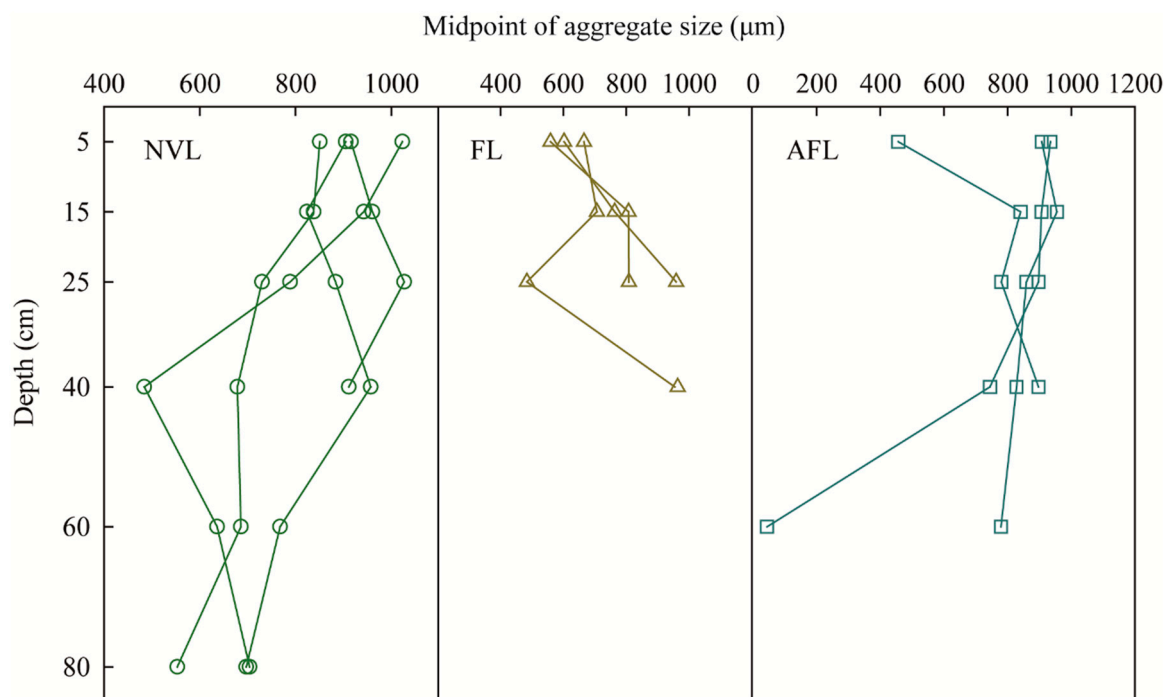


**Figure 4.** The soil aggregate size distributes with depth under native vegetation land (NVL), farmland (FL), and abandoned farmland (AFL).

#### 4. Conclusions

The Grain for Green Project (GGP) has changed the land-use type in the karst area and caused adverse effects, like Hg enrichment in soils. This study has shown that agricultural abandonment can significantly lead to the enrichment of Hg in the soil of the karst region. The THg concentration under different land-use types in the study area increased in the following order: native vegetation land < farmland < abandoned farmland. SOC concentration and macro-aggregates are the most evident contributions of Hg distribution in these types of soil. Macro-aggregates protect SOC, which is the binding agent of Hg, and provide a stable condition to reduce the mobility of Hg in the karst region. Long-term tillage reduces the formation of macro-aggregates in the farmland, resulting in low THg concentration. However, after agricultural abandonment, the macro-aggregates under abandoned farmland gradually recover without tillage disturbance, resulting in the enrichment of Hg in the soil. This study preliminarily explored the effect of GGP on mercury accumulation in soils. Although soil mercury concentrations in the study area were relatively low, the GGP led to mercury enrichment and this consequence should be considered going forward.

**Author Contributions:** Conceptualization, R.Q. and G.H.; methodology, R.Q.; software, R.Q.; validation, G.H.; formal analysis, R.Q.; investigation, G.H.; resources, G.H.; data curation, G.H.; writing—original draft preparation, R.Q.; writing—review and editing, R.Q. and G.H.; supervision, G.H.; project administration, G.H.; funding acquisition, G.H. All authors have read and agreed to the published version of the manuscript.

**Funding:** This research was funded by the National Natural Science Foundation of China, grant number 41661144029 and 41325010.

**Acknowledgments:** We are grateful to Man Liu for field sampling and Qian Zhang for laboratory analysis.

**Conflicts of Interest:** The authors declare no conflict of interest.

## Appendix A

**Table A1.** The data of samples.

Profile	Depth (cm)	THg ( $\mu\text{g}\cdot\text{kg}^{-1}$ )	SOC ( $\text{g}\cdot\text{kg}^{-1}$ )	Proportion (%)		
				Macro-Aggregates	Micro-Aggregates	Silt and Clay
Native vegetation land (NVL)						
NVL1	5	80.60	38.40	76.88	9.41	13.71
NVL1	15	59.30	14.73	76.04	9.18	14.78
NVL1	25	34.50	10.89	69.58	10.61	19.81
NVL1	40	32.30	9.75	66.87	10.95	22.18
NVL1	60	20.80	6.80	67.25	8.83	23.92
NVL1	80	18.90	6.49	61.07	9.72	29.21
NVL2	5	55.20	32.80	80.70	8.84	10.46
NVL2	15	53.70	33.96	75.12	9.49	15.39
NVL2	25	47.90	32.03	79.16	8.42	12.43
NVL2	40	63.90	22.97	84.72	6.88	8.39
NVL2	60	54.30	15.65	71.70	12.88	15.42
NVL2	80	65.70	10.38	67.82	15.51	16.67
NVL3	5	82.30	55.15	81.50	7.81	10.68
NVL3	15	85.50	46.84	85.03	8.61	6.37
NVL3	25	73.90	24.72	90.83	4.65	4.51
NVL3	40	61.00	12.72	81.15	10.86	7.98
NVL4	5	161.40	119.33	90.47	5.58	3.95
NVL4	15	98.50	56.49	83.56	6.20	10.24
NVL4	25	54.80	21.69	72.95	6.80	20.25
NVL4	40	64.70	8.03	58.28	8.27	33.44
NVL4	60	63.00	4.28	64.79	10.26	24.95
NVL4	80	59.90	4.62	68.19	13.58	18.23
Farmland (FL)						
FL1	5	51.70	16.42	61.30	16.93	21.77
FL1	15	41.10	22.85	74.09	11.13	14.78
FL1	25	48.70	24.69	74.15	10.58	15.26
FL2	5	95.20	47.85	63.21	19.27	17.52
FL2	15	54.30	45.77	71.43	15.76	12.81
FL2	25	89.70	53.41	84.86	8.10	7.04
FL3	5	84.70	44.03	66.20	16.52	17.28
FL3	15	82.80	45.54	68.33	18.37	13.30
FL3	25	91.90	46.88	58.27	20.78	20.95
FL3	40	74.70	53.29	84.54	7.93	7.53
Abandoned farmland (AFL)						
AFL1	5	118.10	37.12	82.91	8.02	9.07
AFL1	15	100.00	33.60	80.79	6.76	12.46
AFL1	25	87.20	27.41	80.09	7.90	12.02
AFL1	40	76.80	18.22	70.36	10.94	18.70
AFL1	60	13.00	3.26	26.45	12.67	60.88
AFL2	5	119.60	32.01	80.81	7.11	12.08
AFL2	15	110.60	24.36	84.53	5.61	9.85
AFL2	25	109.40	18.77	77.43	9.88	12.69
AFL2	40	92.30	13.69	75.37	9.19	15.44
AFL2	60	94.40	10.13	72.37	14.15	13.49
AFL3	5	107.80	33.58	57.24	16.36	26.40
AFL3	15	110.50	29.50	76.19	9.22	14.59
AFL3	25	106.10	33.29	72.41	12.36	15.22
AFL3	40	129.40	28.24	80.07	11.07	8.86

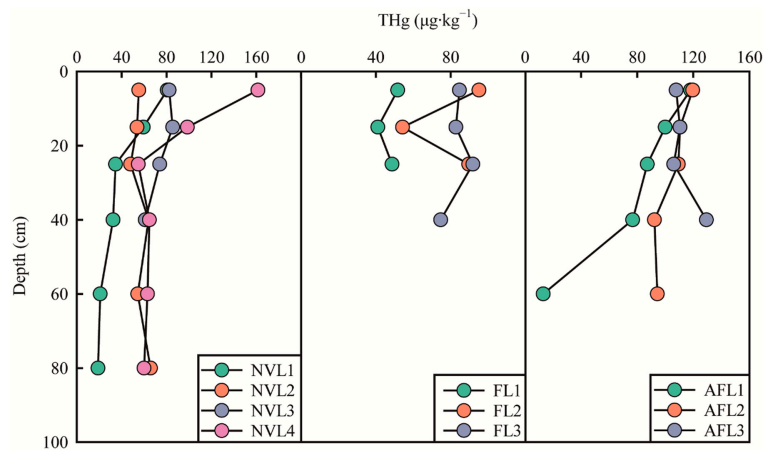


**Figure A1.** The total mercury concentration distributes with depth under native vegetation land (NVL), farmland (FL), and abandoned farmland (AFL).

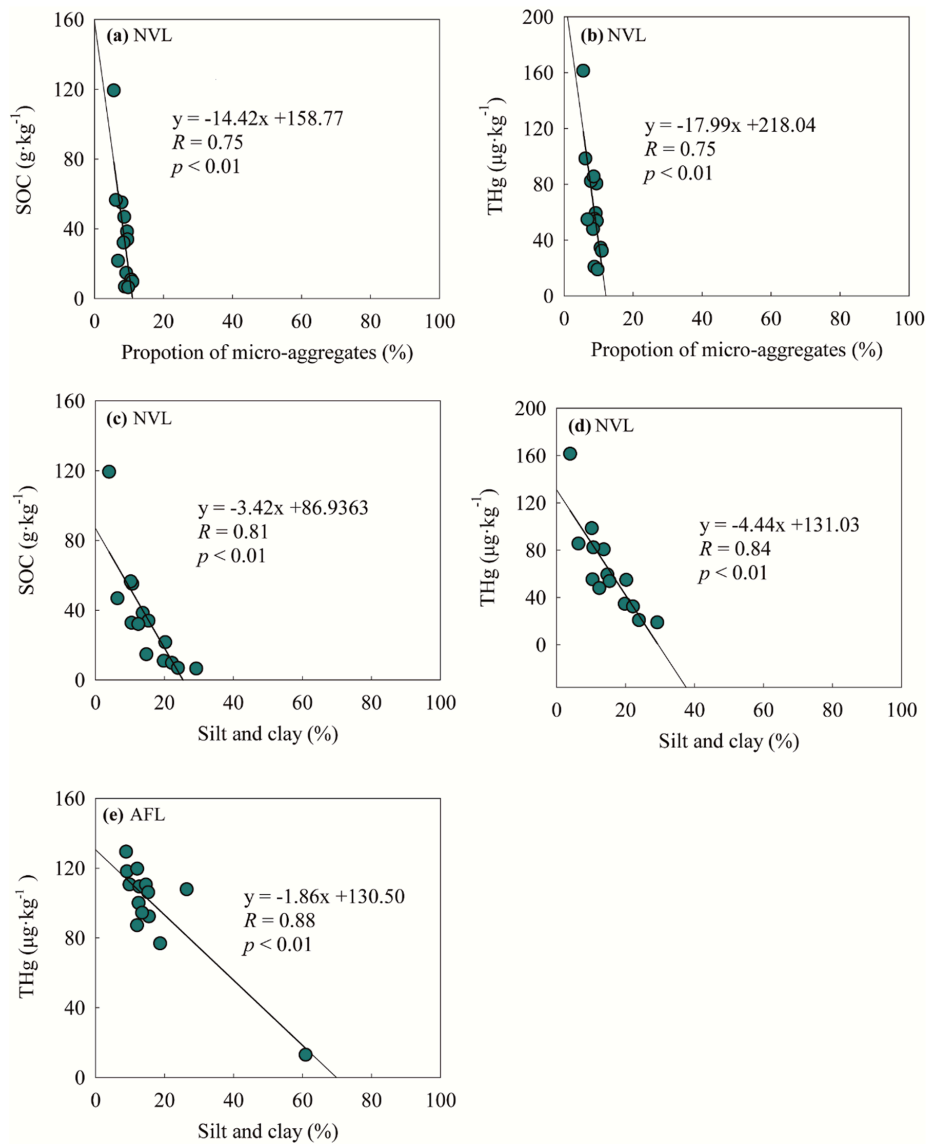


**Figure A2.** Line regression relationships between THg concentration, SOC concentration, the proportion of micro-aggregates, and proportion of silt and clay. NVL: native vegetation land; AFL: abandoned farmland.

## References

1. Liu, Y.; Song, S.; Bi, C.; Zhao, J.; Xi, D.; Su, Z. Occurrence, distribution and risk assessment of mercury in multimedia of Soil-Dust-Plants in Shanghai, China. *Int. J. Environ. Res. Public Health* **2019**, *16*, 3028. [[CrossRef](#)] [[PubMed](#)]
2. Driscoll, C.T.; Mason, R.P.; Chan, H.M.; Jacob, D.J.; Pirrone, N. Mercury as a global pollutant: Sources, pathways, and effects. *Environ. Sci. Technol.* **2013**, *47*, 4967–4983. [[CrossRef](#)] [[PubMed](#)]
3. Bjorklund, G.; Dadar, M.; Mutter, J.; Aaseth, J. The toxicology of mercury: Current research and emerging trends. *Environ. Res.* **2017**, *159*, 545. [[CrossRef](#)] [[PubMed](#)]
4. Teng, D.Y.; Mao, K.; Ali, W.; Xu, G.M.; Huang, G.P.; Niazi, N.K.; Feng, X.B.; Zhang, H. Describing the toxicity and sources and the remediation technologies for mercury-contaminated soil. *RSC Adv.* **2020**, *10*, 23221–23232. [[CrossRef](#)]
5. Zhang, W.; Zhen, G.; Chen, L.; Wang, H.; Li, Y.; Ye, X.; Tong, Y.; Zhu, Y.; Wang, X. Economic evaluation of health benefits of mercury emission controls for China and the neighboring countries in East Asia. *Energy Policy* **2017**, *106*, 579–587. [[CrossRef](#)]
6. Tang, Z.; Fan, F.; Deng, S.; Wang, D. Mercury in rice paddy fields and how does some agricultural activities affect the translocation and transformation of mercury—A critical review. *Ecotoxicol. Environ. Saf.* **2020**, *202*, 110950. [[CrossRef](#)]
7. Yin, R.; Feng, X.; Li, Z.; Zhang, Q.; Bi, X.; Li, G.; Liu, J.; Zhu, J.; Wang, J. Metallogeny and environmental impact of Hg in Zn deposits in China. *Appl. Geochem.* **2012**, *27*, 151–160. [[CrossRef](#)]
8. Selin, N.E. Global biogeochemical cycling of mercury: A review. *Annu. Rev. Environ. Resour.* **2009**, *34*. [[CrossRef](#)]
9. Yan, J.; Wang, C.; Wang, Z.; Yang, S.; Li, P. Mercury concentration and speciation in mine wastes in Tongren mercury mining area, southwest China and environmental effects. *Appl. Geochem.* **2019**, *106*, 112–119. [[CrossRef](#)]
10. Padoan, E.; Romè, C.; Ajmone-Marsan, F. Bioaccessibility and size distribution of metals in road dust and roadside soils along a peri-urban transect. *Sci. Total Environ.* **2017**, *601*, 89–98. [[CrossRef](#)]
11. Sakai, N.; Alsaad, Z.; Thuong, N.T.; Shiota, K.; Yoneda, M.; Mohd, M.A. Source profiling of arsenic and heavy metals in the Selangor River basin and their maternal and cord blood levels in Selangor State, Malaysia. *Chemosphere* **2017**, *184*, 857–865. [[CrossRef](#)] [[PubMed](#)]
12. Tang, Y.; Han, G.L. Characteristics of major elements and heavy metals in atmospheric dust in Beijing, China. *J. Geochem. Explor.* **2017**, *176*, 114–119. [[CrossRef](#)]
13. Lv, J.; Wang, Y. PMF receptor models and sequential Gaussian simulation to determine the quantitative sources and hazardous areas of potentially toxic elements in soils. *Geoderma* **2019**, *353*, 347–358. [[CrossRef](#)]
14. Li, Y.; Zhou, S.; Zhu, Q.; Li, B.; Wang, J.; Wang, C.; Chen, L.; Wu, S. One-century sedimentary record of heavy metal pollution in western Taihu Lake, China. *Environ. Pollut.* **2018**, *240*, 709–716. [[CrossRef](#)] [[PubMed](#)]
15. Fernandez, A.L.; Sheaffer, C.C.; Wyse, D.L.; Staley, C.; Gould, T.J.; Sadowsky, M.J. Associations between soil bacterial community structure and nutrient cycling functions in long-term organic farm soils following cover crop and organic fertilizer amendment. *Sci. Total Environ.* **2016**, *566–567*, 949–959. [[CrossRef](#)]
16. Zeng, J.; Han, G.; Yang, K. Assessment and sources of heavy metals in suspended particulate matter in a tropical catchment, Northeast Thailand. *J. Clean. Prod.* **2020**, *265*, 121898. [[CrossRef](#)]
17. Lal, R. Soil carbon sequestration impacts on global climate change and food security. *Science* **2004**, *304*, 1623–1627. [[CrossRef](#)]
18. Obrist, D.; Johnson, D.W.; Lindberg, S.E.; Luo, Y.; Todd, D.E. Mercury Distribution Across 14 US Forests. Part I: Spatial Patterns of Concentrations in Biomass, Litter, and Soils. *Environ. Sci. Technol.* **2011**, *45*, 3974–3981.
19. Gustin, M.S.; Lindberg, S.E.; Weisberg, P.J. An update on the natural sources and sinks of atmospheric mercury. *Appl. Geochem.* **2008**, *23*, 482–493. [[CrossRef](#)]
20. Poepflau, C.; Don, A.; Vesterdal, L.; Leifeld, J.; Van Wesemael, B.; Schumacher, J.; Gensior, A. Temporal dynamics of soil organic carbon after land-use change in the temperate zone—carbon response functions as a model approach. *Glob. Chang. Biol.* **2011**, *17*, 2415–2427. [[CrossRef](#)]
21. Bachmann, J.; Guggenberger, G.; Baumgartl, T.; Ellerbrock, R.H.; Urbanek, E.; Goebel, M.-O.; Kaiser, K.; Horn, R.; Fischer, W.R. Physical carbon-sequestration mechanisms under special consideration of soil wettability. *J. Plant. Nutr. Soil Sci.* **2008**, *171*, 14–26. [[CrossRef](#)]

22. Han, G.L.; Li, F.S.; Tang, Y. Variations in soil organic carbon contents and isotopic compositions under different land uses in a typical karst area in Southwest China. *Geochem. J.* **2015**, *49*, 63–71. [[CrossRef](#)]
23. Yin, R.; Gu, C.; Feng, X.; Hurley, J.P.; Krabbenhoft, D.P.; Lepak, R.F.; Zhu, W.; Zheng, L.; Hu, T. Distribution and geochemical speciation of soil mercury in Wanshan Hg mine: Effects of cultivation. *Geoderma* **2016**, *272*, 32–38. [[CrossRef](#)]
24. Tisdall, J.M.; Oades, J.M. Organic matter and water-stable aggregates in soils. *J. Soil Sci.* **1982**, *33*, 141–163. [[CrossRef](#)]
25. Liu, C.; Liu, Y.; Guo, K.; Zhao, H.; Qiao, X.; Wang, S.; Zhang, L.; Cai, X. Mixing litter from deciduous and evergreen trees enhances decomposition in a subtropical karst forest in southwestern China. *Soil Biol. Biochem.* **2016**, *101*, 44–54. [[CrossRef](#)]
26. Zeng, J.; Han, G. Preliminary copper isotope study on particulate matter in Zhujiang River, southwest China: Application for source identification. *Ecotoxicol. Environ. Saf.* **2020**, *196*, 110663. [[CrossRef](#)]
27. Liu, J.; Han, G. Effects of chemical weathering and CO<sub>2</sub> outgassing on  $\delta^{13}\text{C}_{\text{DIC}}$  signals in a karst watershed. *J. Hydrol.* **2020**, *589*, 125192. [[CrossRef](#)]
28. Nie, L.; Liu, X.; Wang, X.; Liu, H.; Wang, W. Interpretation of regional-scale distribution of high Hg in soils of karst area in southwest China. *Geochem. Explor. Environ. Anal.* **2018**, *19*, 289–298. [[CrossRef](#)]
29. Parise, M.; De Waele, J.; Gutierrez, F. *Current Perspectives on the Environmental Impacts and Hazards in Karst*; Springer: Berlin/Heidelberg, Germany, 2009.
30. Song, X.; Peng, C.; Zhou, G.; Jiang, H.; Wang, W. Chinese Grain for Green Program led to highly increased soil organic carbon levels: A meta-analysis. *Sci. Rep.* **2014**, *4*, 4460. [[CrossRef](#)]
31. Deng, L.; Liu, G.B.; Shangguan, Z.P. Land-use conversion and changing soil carbon stocks in China's 'Grain-for-Green' Program: A synthesis. *Glob. Chang. Biol.* **2014**, *20*, 3544–3556. [[CrossRef](#)]
32. Deng, L.; Shangguan, Z.-P.; Li, R. Effects of the grain-for-green program on soil erosion in China. *Int. J. Sediment. Res.* **2012**, *27*, 120–127. [[CrossRef](#)]
33. Zhang, K.; Dang, H.; Tan, S.; Cheng, X.; Zhang, Q. Change in soil organic carbon following the 'Grain-for-Green' programme in China. *Land Degrad. Dev.* **2010**, *21*, 13–23. [[CrossRef](#)]
34. Wang, B.; Gao, P.; Niu, X.; Sun, J. Policy-driven China's Grain to Green Program: Implications for ecosystem services. *Ecosyst. Serv.* **2017**, *27*, 38–47. [[CrossRef](#)]
35. Zeng, J.; Han, G. Tracing zinc sources with Zn isotope of fluvial suspended particulate matter in Zhujiang River, Southwest China. *Ecol. Indic.* **2020**, *118*, 106723. [[CrossRef](#)]
36. Zhang, Q.; Han, G.; Liu, M.; Liang, T. Spatial distribution and controlling factors of heavy metals in soils from Puding Karst Critical Zone Observatory, southwest China. *Environ. Earth Sci.* **2019**, *78*, 279. [[CrossRef](#)]
37. Wu, Q.; Han, G.; Tao, F.; Tang, Y. Chemical composition of rainwater in a karstic agricultural area, Southwest China: The impact of urbanization. *Atmos. Res.* **2012**, *111*, 71–78. [[CrossRef](#)]
38. Yang, R.; Zhao, M.; Zeng, C.; Chen, B.; Liu, Z. Spatiotemporal variations of Soil CO<sub>2</sub> in Chenqi, Puding, SW China: The effects of weather and LUCC. In *Hydrogeological and Environmental Investigations in Karst Systems*; Springer: Berlin/Heidelberg, Germany, 2015; pp. 191–205.
39. Han, G.; Li, F.; Tang, Y. Organic matter impact on distribution of rare earth elements in soil under different land uses. *Clean-Soil Air Water* **2017**, *45*, 1600235. [[CrossRef](#)]
40. Zeng, J.; Yue, F.-J.; Wang, Z.-J.; Wu, Q.; Qin, C.-Q.; Li, S.-L. Quantifying depression trapping effect on rainwater chemical composition during the rainy season in karst agricultural area, southwestern China. *Atmos. Environ.* **2019**, *218*, 116998. [[CrossRef](#)]
41. Zhao, M.; Zeng, C.; Liu, Z.; Wang, S. Effect of different land use/land cover on karst hydrogeochemistry: A paired catchment study of Chenqi and Dengzhanhe, Puding, Guizhou, SW China. *J. Hydrol.* **2010**, *388*, 121–130. [[CrossRef](#)]
42. Midwood, A.J.; Boutton, T.W. Soil carbonate decomposition by acid has little effect on  $\delta^{13}\text{C}$  of organic matter. *Soil Biol. Biochem.* **1998**, *30*, 1301–1307. [[CrossRef](#)]
43. Kachurina, O.M.; Zhang, H.; Raun, W.R.; Krenzer, E.G. Simultaneous determination of soil aluminum, ammonium- and nitrate-nitrogen using 1 M potassium chloride extraction. *Commun. Soil Sci. Plant. Anal.* **2000**, *31*, 893–903. [[CrossRef](#)]
44. Han, G.; Tang, Y.; Liu, M.; Van Zwieten, L.; Yang, X.; Yu, C.; Wang, H.; Song, Z. Carbon-nitrogen isotope coupling of soil organic matter in a karst region under land use change, Southwest China. *Agric. Ecosyst. Environ.* **2020**, *301*. [[CrossRef](#)]

45. Liu, M.; Han, G.; Zhang, Q. Effects of agricultural abandonment on soil aggregation, soil organic carbon storage and stabilization: Results from observation in a small karst catchment, Southwest China. *Agric. Ecosyst. Environ.* **2019**, *288*, 106719. [[CrossRef](#)]
46. Li, X.; Han, G.; Zhang, Q.; Miao, Z. Optimal separation method for high-precision K isotope analysis by using MC-ICP-MS with a dummy bucket. *J. Anal. At. Spectrom.* **2020**, *35*, 1330–1339. [[CrossRef](#)]
47. Six, J.; Elliott, E.; Paustian, K.; Doran, J. Aggregation and soil organic matter accumulation in cultivated and native grassland soils. *Soil Sci. Soc. Am. J.* **1998**, *62*, 1367–1377.
48. Qu, R.; Han, G.; Liu, M.; Li, X. The Mercury Behavior and Contamination in Soil Profiles in Mun River Basin, Northeast Thailand. *Int. J. Environ. Res. Public Health* **2019**, *16*, 4131. [[CrossRef](#)]
49. Ding, Z.; Wang, W.; Li, Q.U.; Tang, Q.; Liu, C.; Cheng, J.; Wei, H.U. Mercury Pollution and Its Ecosystem Effects in Wanshan Mercury Miner Area, Guizhou. *Environ. Sci.* **2004**, *25*, 111.
50. Wei, H.; Fan, W.; Wang, X.; Lu, N.; Dong, X.; Zhao, Y.; Ya, X.; Zhao, Y. Integrating supply and social demand in ecosystem services assessment: A review. *Ecosyst. Serv.* **2017**, *25*, 15–27. [[CrossRef](#)]
51. Gao, P.; Niu, X.; Wang, B.; Zheng, Y. Land use changes and its driving forces in hilly ecological restoration area based on gis and rs of northern china. *Sci. Rep.* **2015**, *5*, 11038.
52. Paul, K.I.; Polglase, P.J.; Nyakuengama, J.; Khanna, P. Change in soil carbon following afforestation. *For. Ecol. Manag.* **2002**, *168*, 241–257.
53. Laganier, J.; Angers, D.A.; Pare, D. Carbon accumulation in agricultural soils after afforestation: A meta-analysis. *Glob. Chang. Biol.* **2010**, *16*, 439–453.
54. Nouvellon, Y.; Epron, D.; Kinana, A.; Hamel, O.; Mabilia, A.; D'Annunzio, R.; Deleporte, P.; Saint-André, L.; Marsden, C.; Rouspard, O. Soil CO<sub>2</sub> effluxes, soil carbon balance, and early tree growth following savannah afforestation in Congo: Comparison of two site preparation treatments. *For. Ecol. Manag.* **2008**, *255*, 1926–1936.
55. Six, J.; Elliott, E.T.; Paustian, K. Soil macroaggregate turnover and microaggregate formation: A mechanism for C sequestration under no-tillage agriculture. *Soil Biol. Biochem.* **2000**, *32*, 2099–2103. [[CrossRef](#)]
56. Schlesinger, W.H. Carbon balance in terrestrial detritus. *Annu. Rev. Ecol. Syst.* **1977**, *8*, 51–81. [[CrossRef](#)]
57. Skyllberg, U.; Bloom, P.; Qian, J.; Lin, C.-M.; Bleam, W. Complexation of Mercury(II) in Soil Organic Matter: EXAFS Evidence for Linear Two-Coordination with Reduced Sulfur Groups. *Environ. Sci. Technol.* **2006**, *40*, 4174–4180. [[CrossRef](#)]
58. Hesterberg, D.; Chou, J.; Hutchison, K.; Sayers, D. Bonding of Hg(II) to Reduced Organic Sulfur in Humic Acid As Affected by S/Hg Ratio. *Environ. Sci. Technol.* **2001**, *35*, 2741–2745. [[CrossRef](#)]
59. Qian, J.; Skyllberg, U.; Frech, W.; Bleam, W.; Bloom, P.; Petit, P. Bonding of methyl mercury to reduced sulfur groups in soil and stream organic matter as determined by X-ray absorption spectroscopy and binding affinity studies. *Geochim. Cosmochim. Acta* **2002**, *66*, 3873–3885. [[CrossRef](#)]
60. Dermont, G.; Bergeron, M.; Mercier, G.; Richer-Lafleche, M. Soil washing for metal removal: A review of physical/chemical technologies and field applications. *J. Hazard. Mater.* **2008**, *152*, 1–31.
61. Qu, R.; Han, G.; Liu, M.; Yang, K.; Li, X.; Liu, J. Fe, Rather Than Soil Organic Matter, as a Controlling Factor of Hg Distribution in Subsurface Forest Soil in an Iron Mining Area. *Int. J. Environ. Res. Public Health* **2020**, *17*, 359.
62. Pant, P.; Allen, M. Interaction of soil and mercury as a function of soil organic carbon: Some field evidence. *Bull. Environ. Contam. Toxicol.* **2007**, *78*, 539–542.
63. Palmieri, H.E.; Nalini Jr, H.A.; Leonel, L.V.; Windmüller, C.C.; Santos, R.C.; de Brito, W. Quantification and speciation of mercury in soils from the Tripuí Ecological Station, Minas Gerais, Brazil. *Sci. Total Environ.* **2006**, *368*, 69–78. [[CrossRef](#)] [[PubMed](#)]
64. Cesário, R.; Hintelmann, H.; O'Driscoll, N.J.; Monteiro, C.E.; Caetano, M.; Nogueira, M.; Mota, A.M.; Canário, J. Biogeochemical Cycle of Mercury and Methylmercury in Two Highly Contaminated Areas of Tagus Estuary (Portugal). *Water Air Soil Pollut.* **2017**, *228*, 257.
65. Cesário, R.; Monteiro, C.E.; Nogueira, M.; O'Driscoll, N.J.; Caetano, M.; Hintelmann, H.; Mota, A.M.; Canário, J.o. Mercury and Methylmercury Dynamics in Sediments on a Protected Area of Tagus Estuary (Portugal). *Water Air Soil Pollut.* **2016**, *227*, 475. [[CrossRef](#)]
66. Monteiro, C.E.; Cesário, R.; O'Driscoll, N.J.; Nogueira, M.; Válega, M.; Caetano, M.; Canário, J. Seasonal variation of methylmercury in sediment cores from the Tagus Estuary (Portugal). *Mar. Pollut. Bull.* **2016**, *104*, 162–170. [[CrossRef](#)] [[PubMed](#)]

67. Ruan, Y.; Xiangdong, L.I.; Tinyu, L.I.; Chen, P.; Lian, B. Heavy Metal Pollution in Agricultural Soils of the Karst Areas and Its Harm to Human Health. *Earth Environ.* **2015**, *43*, 92–97.
68. Wang, S.J.; Liu, Q.M.; Zhang, D.F. Karst rocky desertification in southwestern China: Geomorphology, landuse, impact and rehabilitation. *Land Degrad. Dev.* **2004**, *15*, 115–121. [[CrossRef](#)]
69. Liu, M.; Han, G.; Zhang, Q. Effects of soil aggregate stability on soil organic carbon and nitrogen under land use change in an erodible region in Southwest China. *Int. J. Environ. Res. Public Health* **2019**, *16*, 3809. [[CrossRef](#)]
70. Franzluebbers, A.J.; Arshad, M.A. Soil Microbial Biomass and Mineralizable Carbon of Water-Stable Aggregates. *Soil Sci. Soc. Am. J.* **1997**, *61*, 1090–1097. [[CrossRef](#)]
71. Hussain, I.; Olson, K.R.; Wander, M.M.; Karlen, D.L. Adaptation of soil quality indices and application to three tillage systems in southern Illinois. *Soil Tillage Res.* **1999**, *50*, 237–249. [[CrossRef](#)]
72. Li, D.; Zhang, X.; Green, S.M.; Dungait, J.A.J.; Wen, X.; Tang, Y.; Guo, Z.; Yang, Y.; Sun, X.; Quine, T.A. Nitrogen functional gene activity in soil profiles under progressive vegetative recovery after abandonment of agriculture at the Puding Karst Critical Zone Observatory, SW China. *Soil Biol. Biochem.* **2018**, *125*, 93–102. [[CrossRef](#)]
73. Chavarria, D.N.; Pérez-Brandan, C.; Serri, D.L.; Meriles, J.M.; Restovich, S.B.; Andriulo, A.E.; Jacquelin, L.; Vargas-Gil, S. Response of soil microbial communities to agroecological versus conventional systems of extensive agriculture. *Agric. Ecosyst. Environ.* **2018**, *264*, 1–8. [[CrossRef](#)]
74. Rabot, E.; Wiesmeier, M.; Schlüter, S.; Vogel, H.J. Soil structure as an indicator of soil functions: A review. *Geoderma* **2018**, *314*, 122–137. [[CrossRef](#)]



© 2020 by the authors. Licensee MDPI, Basel, Switzerland. This article is an open access article distributed under the terms and conditions of the Creative Commons Attribution (CC BY) license (<http://creativecommons.org/licenses/by/4.0/>).